NATIONAL INSTITUTE OF AEROSPACE

Final Report For:

NASA # NNL04AC40T
TM: M Nurul Abedin

Phototransistor (PT) in the 2 Micron Region

Prepared by:
Dr. Dennis W. Prather
Dr. O. Sulima

National Institute of Aerospace

Development of Phototransistors for the 2-Micron Wavelength Region with Large Photosensitive Area (1000 µm diameter)

**SPONSOR: National Institute of Aerospace**
AWARD No.: DEL-04-01

FINAL REPORT

June 22, 2005 – June 30, 2006

Dr. Dennis W. Prather
Dr. O. Sulima

Within the framework of the project the University of Delaware has developed InGaAsSb-based heterojunction phototransistors (HPT) structure with a large (1000 µm diameter) photosensitive/photoactive area

In comparison with the previous project "Development of Phototransistors for the 2-Micron Region" carried out in 2004-2005, the heterojunction phototransistor structure was optimized. The general HPT mesa structure fabricated and studied in the current project is shown in Fig.1. Two different compositions of quaternary alloys were used to provide the **cutoff wavelength** (50% of maximum quantum efficiency) of **2.4 µm (Type 1)** and **2.15 µm (Type 2)**. The Type 1 HPT was composed of $Al_{0.25}Ga_{0.75}As_{0.02}Sb_{0.98}$ and $In_{0.18}Ga_{0.82}As_{0.17}Sb_{0.83}$ layers with room-temperature bandgaps of $E_g \approx 1.0$ eV and $E_g \approx 0.54$ eV, respectively. The layers are lattice-matched to a GaSb substrate. The growth started with a 0.15µm-thick n+-GaSb buffer layer and was completed with a 0.1µm-thick n+- GaSb contact layer doped with Te. The HPT structure includes a 0.5µm-thick n-type AlGaAsSb emitter, 0.8µm-thick p-type composite base consisting of AlGaAsSb (0.3 µm) and InGaAsSb (0.5 µm) layers, and a 1.5µm - thick n type InGaAsSb collector. The Type 2 HPT differed by a higher bandgap $In_{0.16}Ga_{0.84}As_{0.14}Sb_{0.86}$ layers with a room-temperature bandgap of $E_g \approx 0.555$ eV.
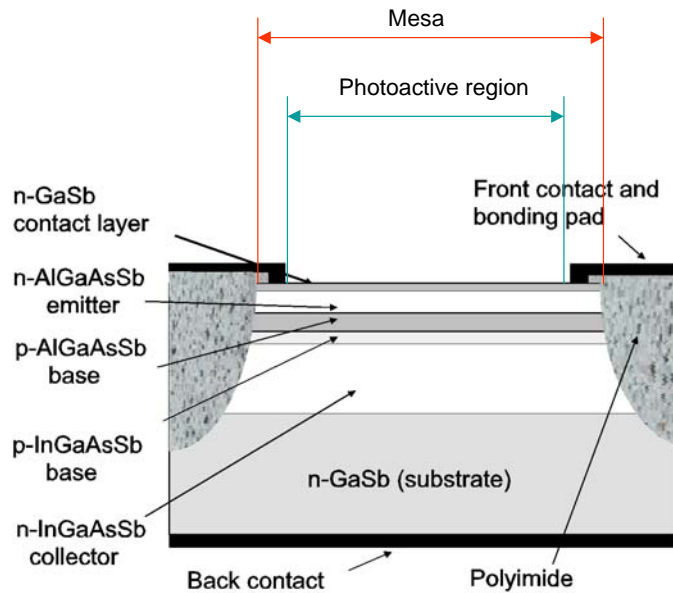

Figure 1.   Structure (cross-section) of AlGaAsSb/InGaAsSb HPTs. Different InGaAsSb compositions were used for Type 1 and Type 2 HPTs.

Fig. 2 shows the picture of an AlGaAsSb/InGaAsSb phototransistor with a 1000 µm diameter of the photosensitive area.

MBE and MOCVD were used for the growth of the Type 1 and Type 2 device structures, respectively. The fabrication process of the mesa HPTs involved photolithography and wet chemical etching. A backside planar and frontside annular ohmic contacts (together with a bonding pad) were deposited by electron-beam evaporation of Au/Ge. A polyimide coating (HD Microsystems PI-2723 photodefinable polyimide resin) was spun on the front of the

device. The polyimide served several functions including planarization of the top surface, mesa isolation, and edge passivation. After dicing, 1-mm² pieces with a single device in the middle of each square were mounted on to TO-18 headers using silver conducting epoxy and wire-bonded. No antireflection coatings were applied.
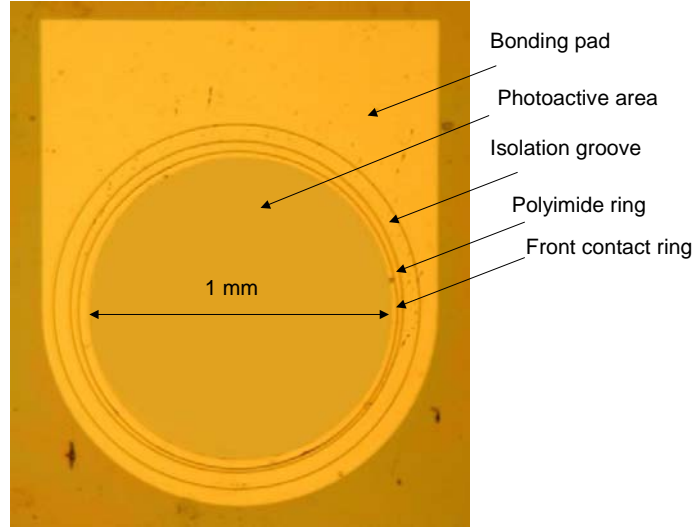
Figure 2.   AlGaAsSb/InGaAsSb HPT with a 1000 μm diameter of the photosensitive area. Mesa diameter is 1100 μm.

This project was the first attempt to fabricate large area photodetectors in the AlGaAsSb-InGaAsSb material system. All earlier publications, as well as our previous project "Development of Phototransistors for the 2-Micron Region" dealt with much smaller devices. One should note that it was not obvious, how the increase of the HPT area (A) will affect its $D*$ or NEP compared to the devices with a smaller area. On one hand, one can expect higher $D*$ due to $D* \propto A^{0.5}$. On the other hand, a larger area of the device will inevitably lead to an increase of dark current I_d, and hence to a decrease of $D*$ due to the following dependencies:

$$D*(A) = R\sqrt{A}/I_n(A) \text{ and}$$
$$I_n \propto \sqrt{I_d(A)}$$

In addition - if quality of the wafer used for HPT fabrication is not perfect - probability of device random defects (e.g. crystal defects like precipitates) leading to shunts and hence higher I_d is higher at a larger area. Moreover, as $D*$ increases through a larger photosensitive area and decreases through a larger mesa area (see Fig. 1), the ratio between these two areas is of importance.

To determine the influence of the device area on device parameters, HPTs with three different diameters of photoactive (value of the numerator below) and mesa (value of the denominator below) regions were fabricated and studied: **A – 75 μm / 125 μm, B – 200 μm / 300 μm, and C – 1000 μm / 1100 μm**. Ratios between photoactive areas and total/mesa areas are 0.36 (A), 0.44 (B) and 0.84 (C).

3

Fig. 3 shows room-temperature dark J-V characteristics (reverse bias only) of Type 1 HPTs with different designs (A, B, C) made of two epitaxial wafers (#331 and # 401). One can see that at a low bias (< 0.25 V), the large devices (design C) exhibit the lowest current densities. At higher voltages, the minimum J depends on design, wafer used and the voltage range.
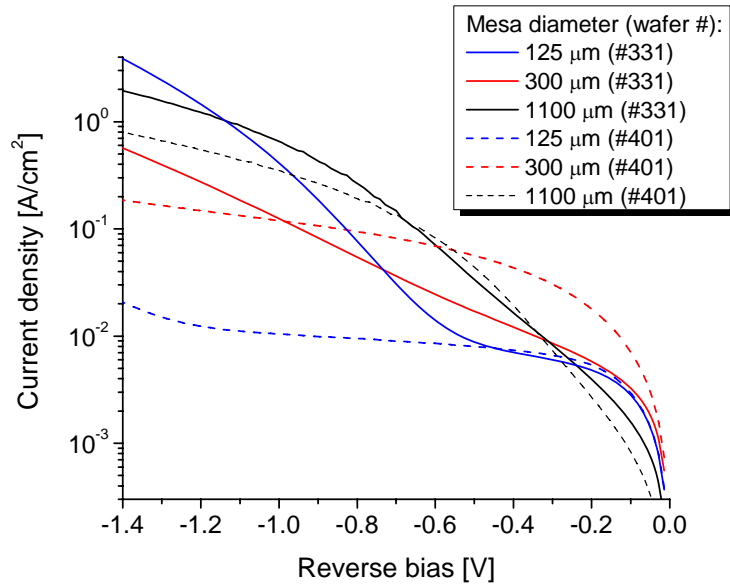

Figure 3. Room-temperature dark J-V curves of MBE-grown HPT of Type 1 with different designs (A, B, C) made of two epitaxial wafers (#331 and # 401).

This rather complicated dependence and relatively large difference between different epitaxial wafers was – to large extent – caused by a relatively low crystal quality of the MBE-grown wafers. This can be explained by a very complicated growth procedure, which required more optimization.

Structural parameters of device structures, including lattice mismatch and crystalline perfection, have been characterized by high-resolution x-ray diffraction in a triple-crystal arrangement. Analysis of 2Θ-ω and ω Coherent Rocking Curves and Reciprocal Space Maps allowed determining the type and spatial distribution of crystalline defects.

As an example, Fig. 4 shows x-ray diffraction patterns, measured at different parts of the sample #401. Additionally, Fig. 5 shows a Reciprocal Space Map of the same sample in one of its points. One can see that there is a relatively large distance between GaSb, InGaAsSb and AlGaAsSb peaks (lattice mismatch) as well as elongation of the main diffraction spots in Δω direction, which may be the cause of point crystalline defects threading and misfit dislocations.
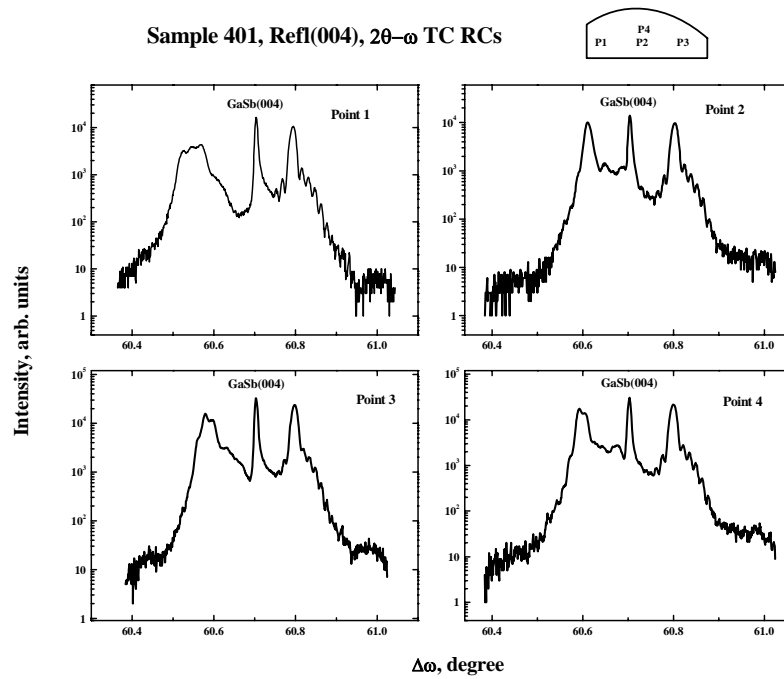
Figure 4. X-ray diffraction patterns measured at different parts of the Type 1 sample #401.

Sample 401, Point 4, TC RSM, Refl(004)
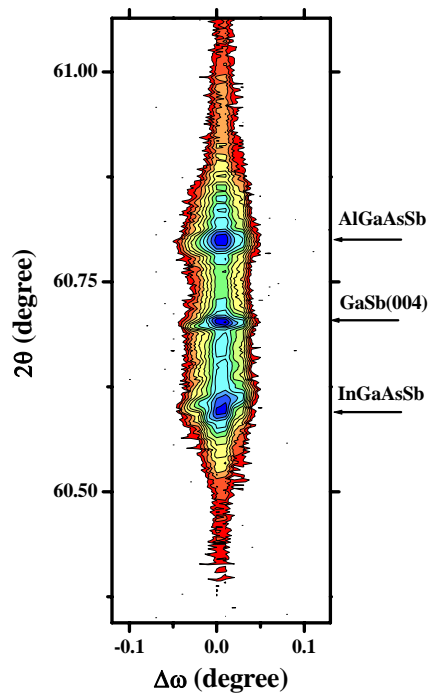
**Figure 5**. Reciprocal Space Map measured on the Type 1 sample #401.

5

Nevertheless, we managed to fabricate HPT of these wafers, which showed decent characteristics.

Fig. 6 shows spectral response of an MBE-grown AlGaAsSb/InGaAsSb phototransistor (Type 1, Design B) at the specified bias voltage and +20°C. As can be seen in Fig.6, responsivity R rapidly increases with applied bias voltage and at 1.4 V reaches 1128 A/W for λ = 2.04 - 2.08μm, which is the wavelength range of interest for the current project. Even higher values of R (up to 2334 A/W) were measured at -20°C at 1.4 V for λ = 2.05 μm.

Fig. 7 shows responsivity R of an AlGaAsSb/InGaAsSb phototransistor (Type 1, Design B) at λ = 2.05 μm vs. bias voltage at temperatures from -20°C to +100°C. One can distinguish two parts of the graph: at very low voltage (< 1V) higher R was measured at higher temperatures, while at higher voltages the opposite dependence was observed. This complicated behavior can be explained by temperature dependencies of minority-carrier (electrons) diffusion length in the base, and by the as-yet-unexplored temperature-sensitive band discontinuities of AlGaAsSb/InGaAsSb heterojunctions, which can affect the minority carrier injection at the emitter-base junction and consequently the gain of the phototransistor.
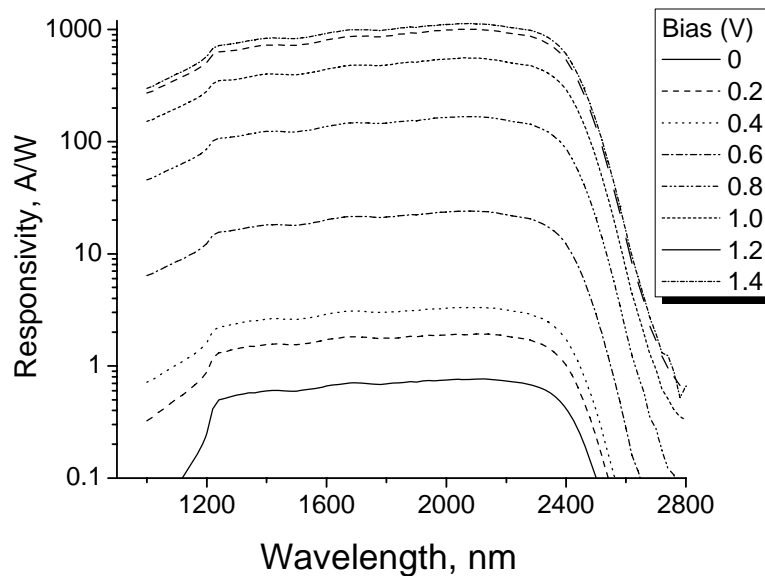
Figure 6.   Spectral response of an MBE-grown AlGaAsSb/InGaAsSb phototransistor (Type 1, Design B) at the specified bias voltage and +20°C. The measurements were carried out at NASA Langley Research Center.
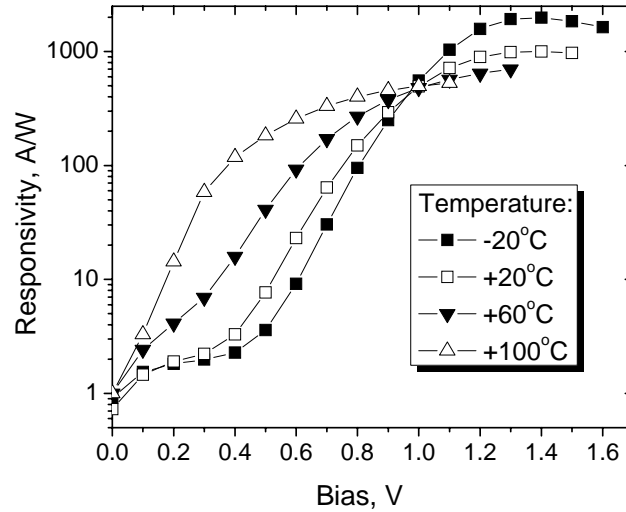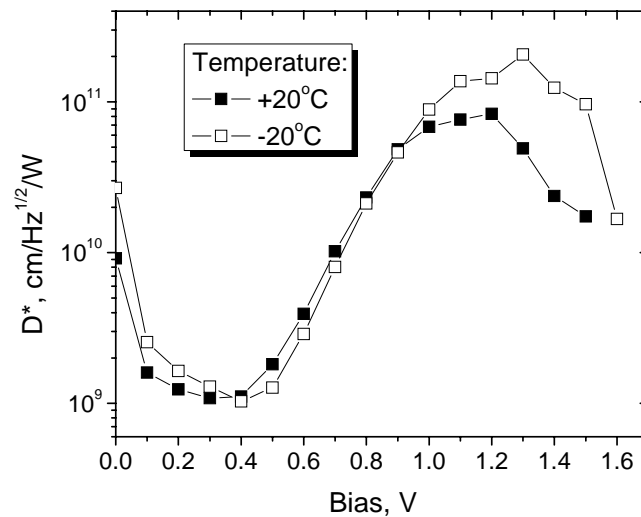
Figure 7.   Responsivity of an MBE-grown AlGaAsSb/InGaAsSb phototransistor (Type 1, Design B) at $\lambda = 2.05$ μm vs. bias voltage at specified temperatures. The measurements were carried out at NASA Langley Research Center.

On the other hand, the dark current and hence the noise current I_n of the phototransistor are also dependent on applied voltage and temperature. All the above dependencies are considered in specific detectivity D^*, which is one of the main figures of merit for any photodetector:

$$D^*(T,V) = R(T,V) \cdot \sqrt{A}/I_n(T,V) \tag{1}$$

where A is the detector area.

Fig. 8 exhibits a 2.05-μm detectivity D^* of an AlGaAsSb/InGaAsSb phototransistor at −20ºC and +20ºC vs. bias voltage. D* value as high as 2.1×10^{11}cmHz$^{1/2}$/W was determined at −20ºC and 1.3 V. This is equivalent to a noise-equivalent-power of 1.3×10^{-13} W/Hz$^{1/2}$.

**Figure 8**.   A 2.05-μm detectivity D* of an MBE-grown AlGaAsSb/InGaAsSb phototransistor (Type 1, Design B) at −20ºC and +20ºC vs. bias voltage. The measurements were carried out at NASA Langley Research Center.

7

However, due to the above problems with the insufficient crystal quality, it was possible to fabricate Type 1 devices only with a relatively small photosensitive area (Design A and B). Owing to a relatively high density of crystal defects, the noise of the larger devices (Design C) was too high.

Compared to the MBE-grown wafers, better results in terms of crystalline quality were achieved by using MOCVD for Type 2 devices. This fact was extremely important for fabrication of high-quality HPTs with a large area (Design C).

As an example, Fig. 9 shows an x-ray diffraction pattern, measured on a MOCVD-grown sample. Additionally, Fig. 10 shows a Reciprocal Space Map of the same sample. One can see that compared to Figs. 4 and 5 much higher crystalline quality was achieved, resulting in less dislocations and point defects.

Sample # VE640B, Center, GaSb(001)-TS, TC 2θ−ω RC, Refl(004)
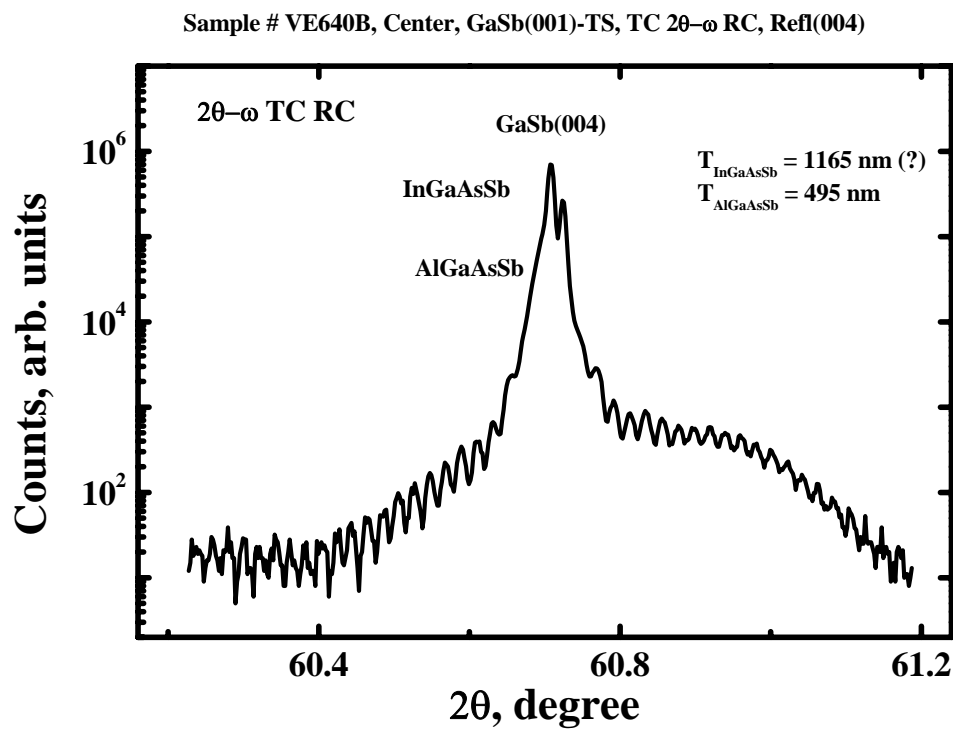
Figure 9.   X-ray diffraction pattern measured on a MOCVD-grown sample of Type 2.

**Sample # VE640B, Center, TC RSM, Refl(004)**
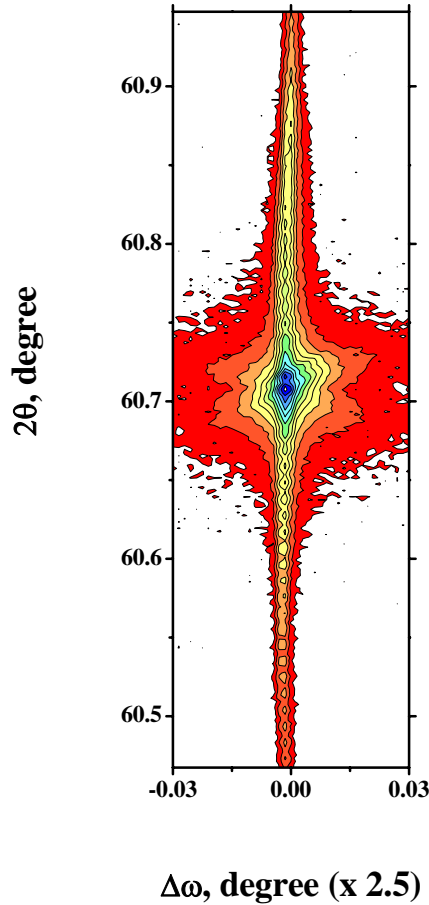
Figure 10.   Reciprocal Space Map measured on a Type 2 MOCVD-grown sample.

Fig. 11 shows room-temperature dark J-V characteristics (reverse bias only) of Type 2 HPTs with designs B and C. One can see that at a low bias (< 0.6 V), the large devices (design C) exhibit the lowest current densities. One should note (see below) that the operational voltage of this type of devices is < 0.6 V, and hence – when the high crystal quality of the epitaxial wafers is provided - larger devices are preferable to the smaller ones in terms of D* or NEP.

Fig. 12 underlines the difference between the dark current densities (and hence noise) of the devices with the same design (C), but different types. To large extent, this difference can be explained by a essentially better crystalline quality of the MOCVD-grown wafers.
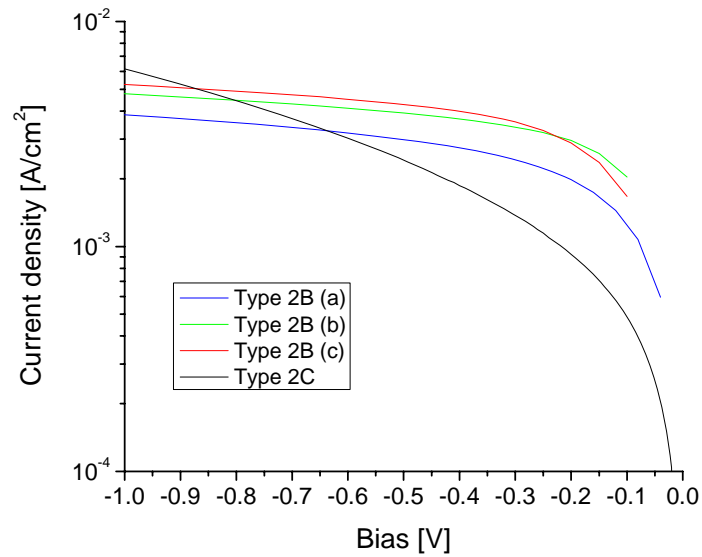
Figure 11.   Room-temperature dark J-V curves of MOCVD-grown HPT of Type 2 with designs B (three devices) and design C.
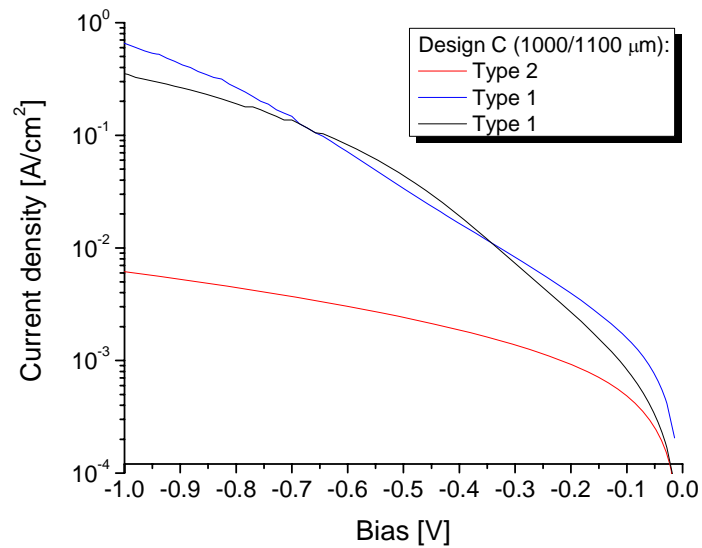
Figure 12.   Room-temperature dark J-V curves of the HPT of the same design C (1000/1100 μm), but different types.

Thus, we have demonstrated that HPTs with a large area can exhibit a lower dark current density compared to smaller devices.

Due to a high crystal quality, these devices demonstrated excellent quantum efficiency. Fig. 13 shows the quantum efficiency of a Type 2 (C) HPT, measured at NASA LaRC at $+20^{o}C$ and $-10^{o}C$.

10
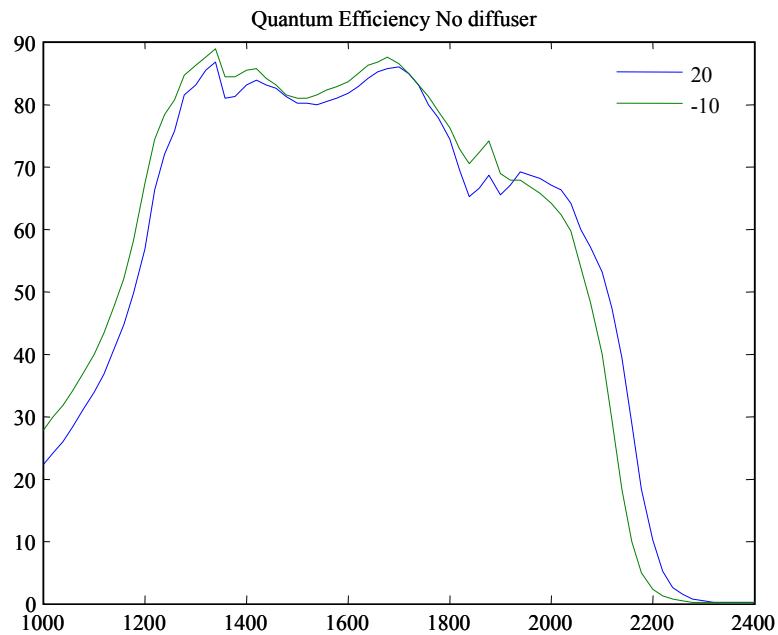
Figure 13.   Spectrum (wavelength in nm) of quantum efficiency (in %) of a Type 2 (C) HPT (#10-1-A1), measured at NASA LaRC at +20°C and –10°C.

Fig. 14 shows spectral response of an MOCVD-grown HPT (Type 2, Design C) at the specified bias voltage and +20°C.
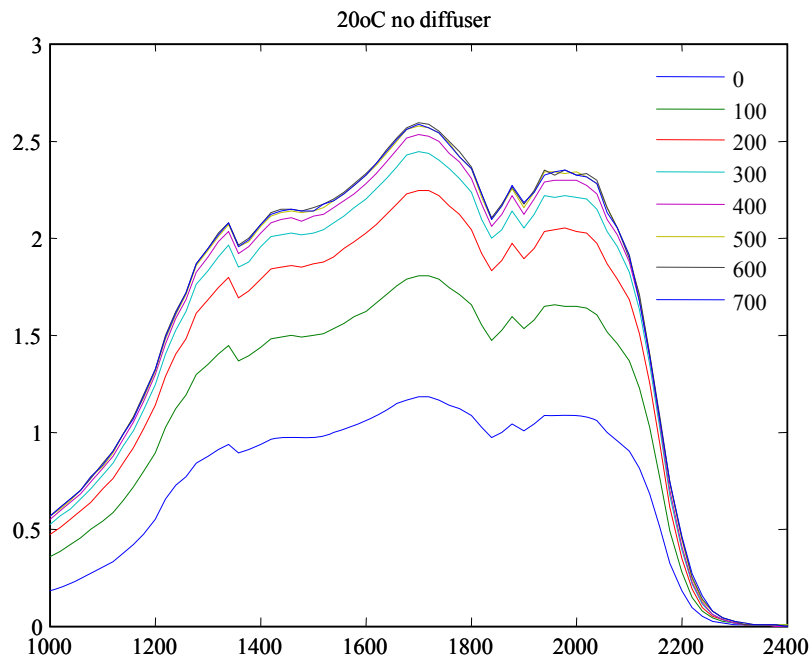

Figure 14.   Spectral response of responsivity (A/W) of a Type 2 (C) HPT (#10-1-A1), measured at NASA LaRC at +20°C.

Based on these results, NASA LaRC calculated NEP of the 1-mm HPTs to be about 10^{-13} W/Hz$^{1/2}$ at 20C and zero bias, which corresponds to D* $\approx 10^{11}$ cm Hz$^{1/2}$/W. These values are substantially better than previously record parameters of the 200- μm LPE-grown HPTs at

11

the same measurement conditions. Even better results are expected at low reverse bias and lower temperatures.

On the other hand, it is obvious that for minimizing noise and capacitance, small area devices are preferable. Therefore, it could be beneficial to replace large-area HPTs by small-area ones with integrated optical lenses (e.g. diffractive optic elements - DOE), which allow keeping the spectral response at the level of large-area devices. The University of Delaware has experience in developing approaches for such integration. In the context of the current proposal, DOE optimized for the wavelength of interest could be integrated with HPTs. DOEs are surface relief patterns etched into an optical substrate that redirect and focus light through the mutual interference of propagating waves. DOEs have low f-number and very high-diffraction efficiency.

Fig. 15 shows a scheme of the HPT integration with a DOE. In this work the first 300-μm diameter photoresist-on-glass DOEs were specially designed and fabricated for the integration with the HPTs. In particular, HPTs with a 75 μm diameter of the photosensitive area (design A) were integrated with the 300-μm DOEs. Integration of the HPT and DOE was performed according to Fig. 15.
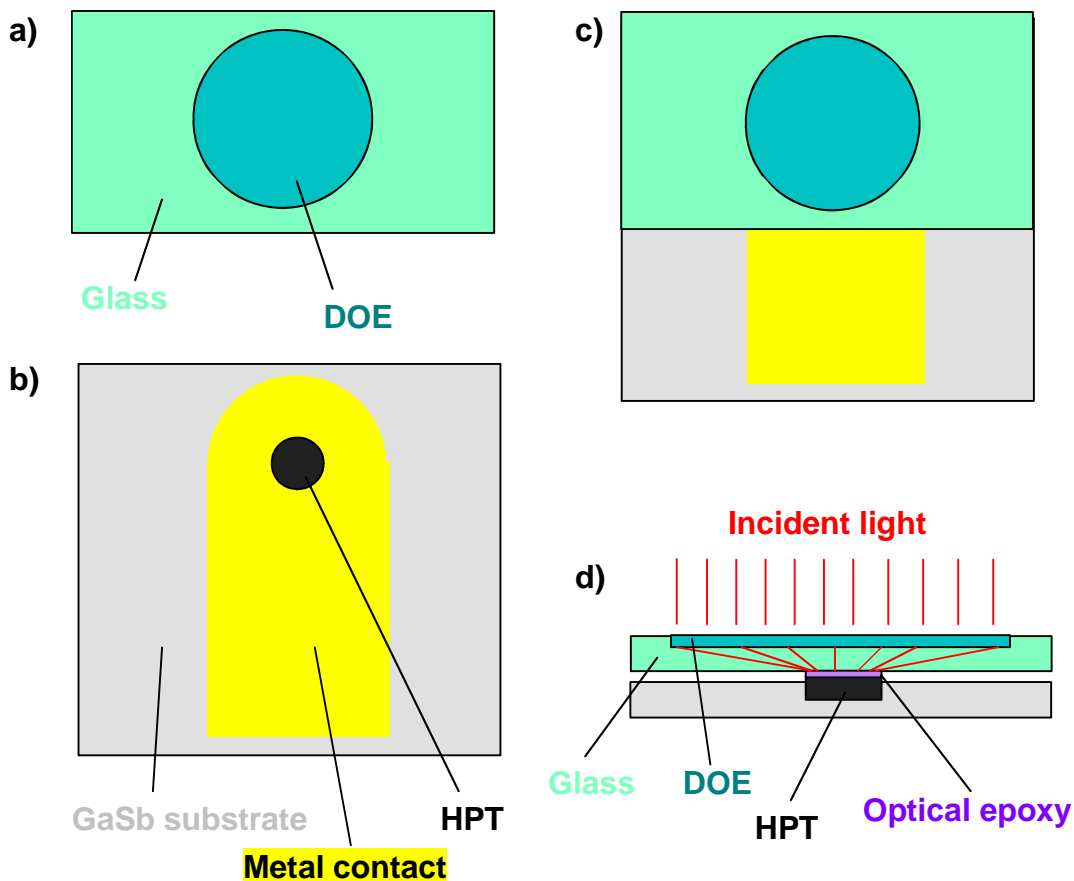
Figure 15. Schematic of HPT integration with a DOE: a) DOE on glass; b) HPT on GaSb substrate; c) HPT-DOE integration (top view); d) HPT-DOE integration (cross-section)
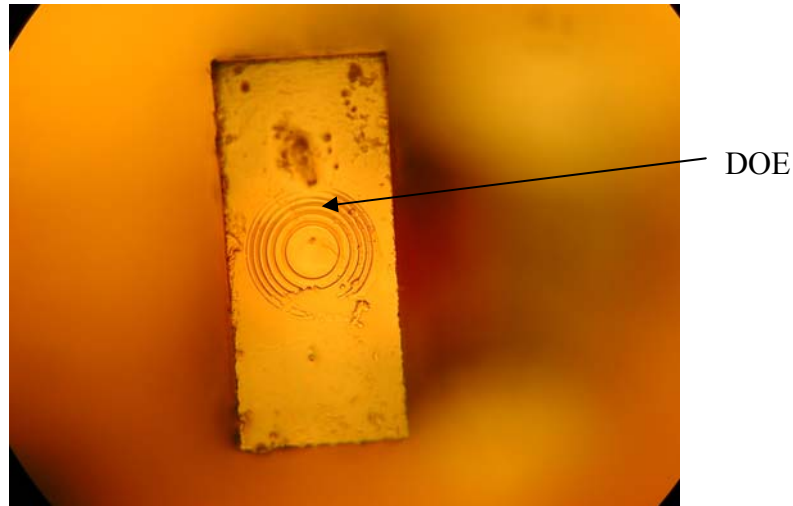
Figure 16. Picture of the first 300-μm diameter photoresist-on-glass DOE designed and fabricated for a 75-μm HPT.

Fig.16 demonstrates some visible defects on the DOE surface. Despite the defects, a strong (3-6 times) increase of the spectral response has been already measured for the integrated structure (see below). However, we believe that the quality of the DOE can be significantly improved. Thus, there is a potential for further improvement of the HPT parameters through better DOEs.

Fig.17 shows a cross-section of the integrated DOE-HPT structure. Optical epoxy was used for the optical connection of the DOE with the HPT.
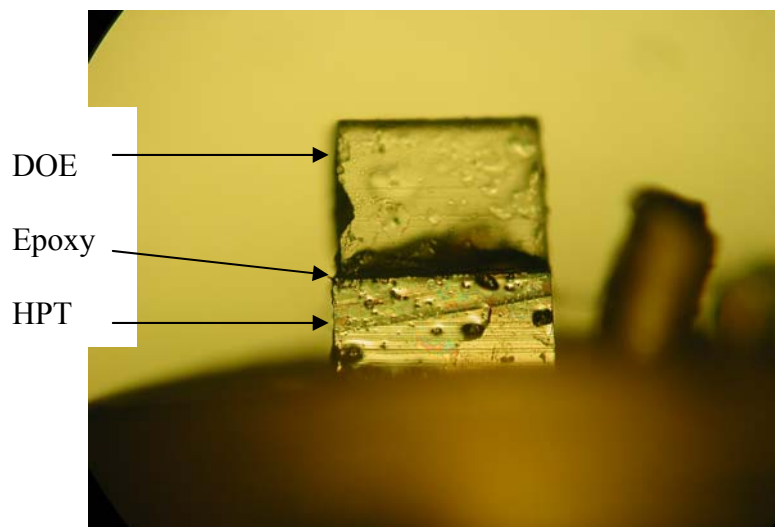
**Figure 17.** Cross-section of the integrated DOE-HPT structure.

To determine the optical efficiency of the DOE, spectral response (SR) measurement of the HPT were performed before and after integration. Fig.18 shows SR curves measured at

different bias voltages. One can see a significant (3-6 times) improvement of the SR due to the application of the DOE.
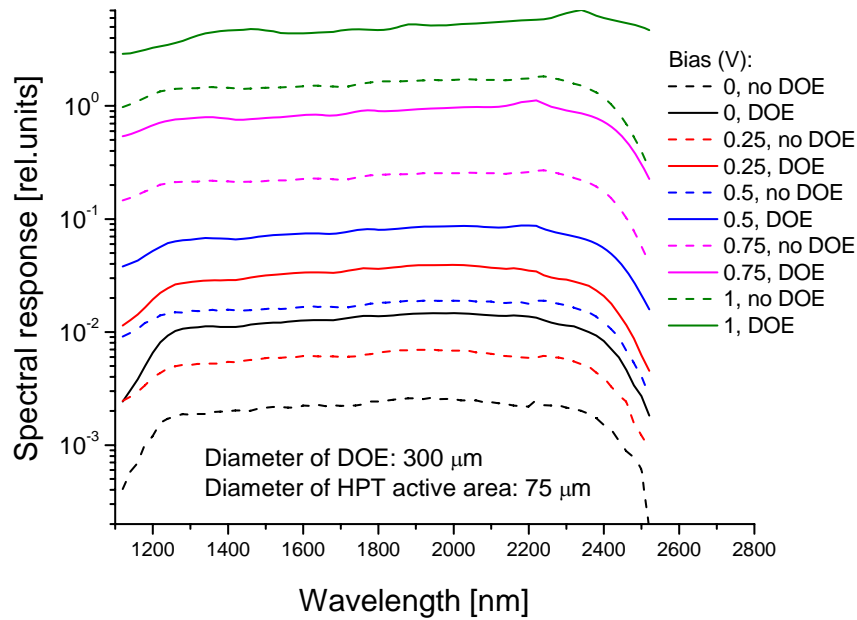
Figure 18. Room-temperature spectral response of AlGaAsSb/InGaAsSb 75-μm diameter HPTs (design A) before and after integration with a 300-μm DOE. Different bias voltages were applied.

Fig.19 shows the ratio of SR of the HPT before and after integration with the DOE. One can see that this ratio is in the range of 3 - 6.
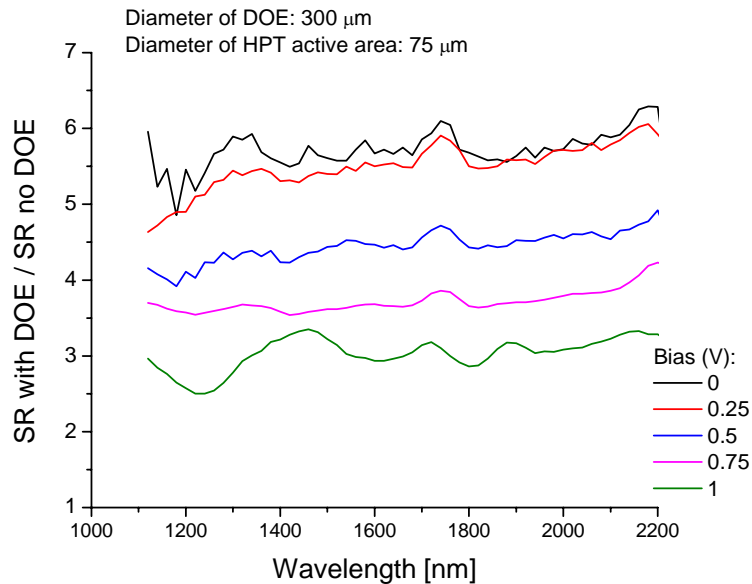
Figure 19. Ratio of SR of the HPT vs. wavelength at various bias voltages before and after integration with the DOE.

Taking into account the ratio of the DOE and the HPT diameters (300 μm and 75 μm), one could expect the maximum SR increase of 16, provided the optical efficiency of the DOE is 100%. We believe, that due to a better understanding of the DOE fabrication and getting more experience, we will achieve the DOE optical efficiency of about 80-85%. Thus, one can expect a 10-fold improvement of the SR for the HPTs and DOEs of the above sizes.

Conclusions:

1. The first MBE- and MOCVD-grown AlGaAsSb/InGaAsSb heterojunction phototransistor structures were demonstrated, tested and optimized.
2. Large-area low-voltage AlGaAsSb/InGaAsSb heterojunction phototransistors with the diameter of the photosensitive area 1 mm were fabricated, characterized and delivered to NASA Langley Research Center.
3. The HPTs demonstrated excellent quantum efficiency exceeding 65% at 2-μm at $+20^{\circ}$C and -10°C.
4. NASA LaRC calculated NEP of the 1-mm HPTs to be about 10^{-13} W/Hz$^{1/2}$ at $+20^{\circ}$C and zero bias, which corresponds to D* $\approx 10^{11}$ cm Hz$^{1/2}$/W. These values are substantially better than previously record parameters of the 200- μm LPE-grown HPTs at the same measurement conditions. Even better results are expected at low reverse bias and lower temperatures.
5. The first successful DOE-HPT integration focused on further minimization of noise and capacitance of HPTs was demonstrated. The increase of spectral response and hence D* is 3-6 times for the 300-μm DOE and 75-μm HPT.